Check for updates

A new technique of quantifying protoporphyrin IX in microbial cells in seawater

Lide Gu[1,2], Xinli Yue[1,2], Haowen Zhong[1,2], Kang Mei[1,2] and Deli Wang[1,2]*

[1]State Key Laboratory of Marine Environmental Science, Xiamen University, Xiamen, China,
[2]College of Ocean and Earth Sciences, Xiamen University, Xiamen, China

Protoporphyrin IX (PPIX), a fundamental precursor in the synthesis of heme and chlorophyll, plays a vital role in the biological metabolism and biogeochemical cycling in the ocean. PPIX has previously been identified in humans, animals, and plants, while so far as we know, there is no measurements until now regarding its contents in microbes, and especially in marine phytoplankton and bacteria. Here, for the first time, we reported a method of determining PPIX in marine microbial cells *via* acetone extraction followed by reversed phase high-performance liquid chromatography quantification, in which acetone-acetonitrile/water-formic acid buffer was used as a gradient elution solvent. The method was optimized with the detection limit of 3.8 ± 1.0 pM, and recovery rate of $97.5 \pm 1.9\%$. The structure of the extracted PPIX was further confirmed using tandem mass spectrometry as positively associated with specific protonated molecules $[M + H]^+$. The method was then successfully applied in the determination of PPIX in microbial cells in the water samples collected from a median-sized subtropical estuary (the Jiulong River Estuary, China). The results showed that PPIX existed widely and ranged from $20 - 170$ ng/L in cells in the water samples. In the whole estuary, cellular PPIX generally decreased linearly with increasing salinity. A positive correlation of PPIX with particulate organic matter in the estuary suggested of sediment suspension and dissolution as its possible source. In addition, a general hyperbolic fitting pattern was observed for PPIX against dissolved inorganic nitrogen, PO_4^{3-}, and the bacterial abundance ($10^4 - 10^6$ cells/mL) in the estuary. Such results indicated that PPIX played a crucial role in linking nutrients and the microbial productivity. In summary, we developed a new technique of quantifying cellular PPIX in water samples and confirmed the wide existence of cellular PPIX in natural waters. The data from Jiulong River estuary further suggest that the contents of cellular PPIX be enhanced with the nutrient supply from riverine inputs and sediment suspensions, which thereafter dictate the productivity of phytoplankton and bacteria in coastal waters.

Introduction

Protoporphyrin IX (PPIX) is an essential precursor with some specific physiological functions such as oxygen transport and storage mediated by heme (iron/zinc-PPIX) or hemocyanin (copper-PPIX) and photosynthesis by chlorophyll (magnesium-PPIX). It is also a ubiquitous prosthetic group of proteins such as cytochrome, catalases, peroxidases, and nitrate reductase (Xiong et al., 2011; Senge et al., 2014; Sachar et al., 2016). Consequently, PPIX participates in fundamental metabolic processes in cells and plays a vital role in cell biology. PPIX is an endogenous fluorescent heterocyclic organic molecule, and its biosynthesis includes eight key enzymatic processes in the mitochondria and cytoplasm of cells (Sachar et al., 2016). Figure 1 shows the proposed biosynthetic pathway of PPIX in the cells of mammals, fungi, yeasts, and the α-subgroup of proteobacteria, which starts from source materials: glycine and succinyl-CoA (Sachar et al., 2016). Alternatively, PPIX is initiated from glutamate and tRNA in plants, green algae, cyanobacteria, archaea, and most bacteria (Senge et al., 2014). All the synthesizing processes are dictated from strict enzymatic reactions under specific environmental conditions (Bonkovsky et al., 2013). Thus, any disturbance in these steps might cause an accumulation of or deficiency in intracellular PPIX, and even lead to severe porphyria (Dailey and Meissner, 2013). It has been reported that extra supply of nitrogen nutrients might seriously affect the formation of proteins including synthetase, reductase, and aminomutase, as well as the porphyrin rings. On the other hand, lack of necessary carbon compounds hindered the tricarboxylic acid (TCA) cycle and thus affected the production of succinyl-CoA, and influenced the porphyrin synthesis (Kaneko, 2008). Similarly, lack of phosphorus also interfered the biological energy and material cycling in the marine ecosystem (Tian et al., 2021). In addition, endogenous metabolites could dictate the eukaryotic and prokaryotic members of a microbial community *via* complex ecological interaction between producers and auxotrophs (Chen et al., 2018). These specific biomolecules might play a critical role in modulating the ecological systems, and even linking the global biogeochemical cycles (Suffridge et al., 2018).

PPIX has previously been detected by using a series of techniques including the fluorometry (Datta et al., 1998), thin-layer chromatography (De Maere et al., 2014), capillary electrophoresis (Weinberger and Sapp, 1990), and the high-performance liquid chromatography (HPLC) coupled with mass spectrometry (MS) (Fyrestam et al., 2015; Fyrestam and Östman, 2017). Mass spectrometry provides structural information, and HPLC is used for precise quantification. HPLC-MS has become a reliable technique for measuring PPIX recently due to its high precision and accuracy (Lim; Zvezdanovic et al). Previous analyses of PPIX mainly focused on samples taken from human, such as the urines (Ausio et al., 2000), blood, and

feces (Danton and Lim, 2006), and there were only a few published data available regarding microorganisms. For example, Fyrestam et al. firstly determined a porphyrin profile of *Aggregatibacter actinomycetemcomitans* in oral biofilms by using the HPLC/MS method (Fyrestam et al., 2015). In addition, the PPIX contents have also been reported in some plants and algae (Stillman LC, 1978; Weinstein JD, 1984; Espinas et al., 2012). Although important, the currently available PPIX studies focused primarily on its applications in human health, industrial development, or single-tissue testing. There is still no records of PPIX measurements in natural environments so far. We are still lack of studies on its ecological functioning in microbial communities, and especially in marine ecosystems. Therefore, there is a need of establishing a reliable and accurate method for extracting and quantifying PPIX in natural samples. This study aimed to develop such a method to determine cellular PPIX in estuarine and coastal waters. Along with its post-derivatives (chlorophyll, pheophytin, and bacteriochlorophyll), we expect that this new analytical protocol will allow for a preliminary understanding of the cycling of PPIX in natural environment, and its roles in mediating global marine biogeochemical cycles and the succession of microbial species.

Methods

Chemicals and materials

The protoporphyrin IX (purity ≥ 95%), chlorophyll-*a*, and bacteriochlorophyll-*a* were obtained from Merck (Darmstadt, Germany). The HPLC-grade acetonitrile, acetone, and formic acid (≥ 98%) were also purchased from Merck. The InertSustain C18 column (4.6 × 150 mm, 5 μm) was sourced from GL Science (Tokyo, Japan). A Milli-Q Element water purification system from Millipore (USA) was used to produce deionized water at 18.2 MΩ cm. The 0.45 μm Millipore organic needle filters were from Merck, and the 1.5 mL sample vials were from CNW Technologies GmbH (USA). The 0.7 μm and 47 mm GF/F filters were from Whatman (UK). All of the other inorganic chemicals and organic solvents used in the study were of analytical grade.

Environmental settings of study area

The Jiulong River is the 13th largest river in China with an average annual total freshwater discharge of 1.47×10^{10} m^3. The Jiulong River is located in a highly populated area in Southeast China with influences from agricultural, industrial, and municipal activities nearby (Wang et al., 2018). The Jiulong River estuary (JRE) is a typical subtropical macrotidal estuary, and subject to human perturbation within the whole estuary (Figure 2). The Jiulong River
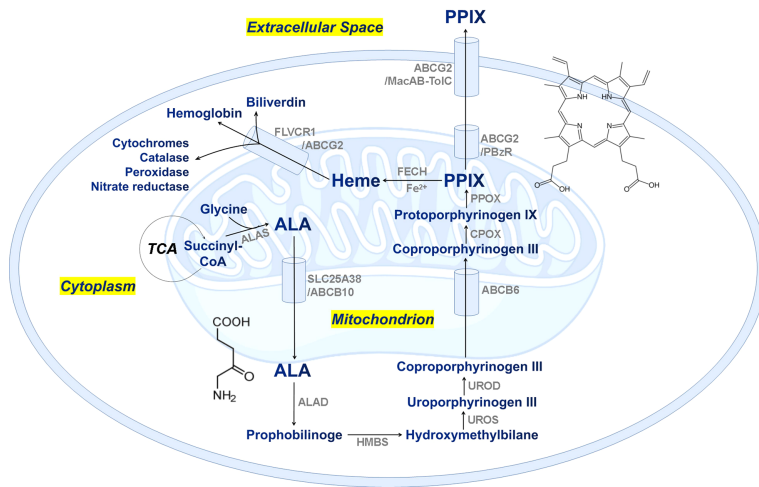
FIGURE 1

The proposed biosynthetic pathway of PPIX/heme in mammalian cells. TCA, tricarboxylic acid cycle; ALA, δ-aminolevulinic acid; ALAS, ALA synthase; SLC25A38, solute carrier family 25 member 38; ABCB, ATP-binding cassette subfamily B member; ALAD, ALA dehydratase; HMBS, hydroxymethylbilane synthase; UROS, uroporphyrinogen III synthase; UROD, uroporphyrinogen decarboxylase; CPOX, coproporphyrinogen oxidase; PPOX, protoporphyrinogen oxidase; ABCG2, ATP-binding cassette subfamily G member 2; FECH, ferrochelatase; FLVCR1, feline leukemia virus subgroup c receptor 1; MacAB-TolC, an efflux pump involved in *E. coli* and *Salmonella* for macrolide efflux.

estuary could be divided into three parts geochemically: the upper, lower estuaries and the bay areas. The upper estuary receives a large amount of inputs of terrestrial materials from the river, and the lower estuary is subject to strong tidal intrusion with sediment disturbances locally. The bay area is surrounding the Xiamen Island, with a low oxygen zone and even algal bloom occurring occasionally (Chen et al., 2019; Baohong et al., 2021).

Sample collection and processing

The water samples used for quantifying PPIX were collected from the surface (~ 0.5 m below) and bottom (~ 1 m above) in the JRE on 14th – 15th November 2021 (Figure 2). Totally, thirty-two water samples were taken at 16 stations, and the values of salinity increased gradually from 0 ~ 32 from the upper to lower estuaries (stations of A3-JY3), and afterwards remained
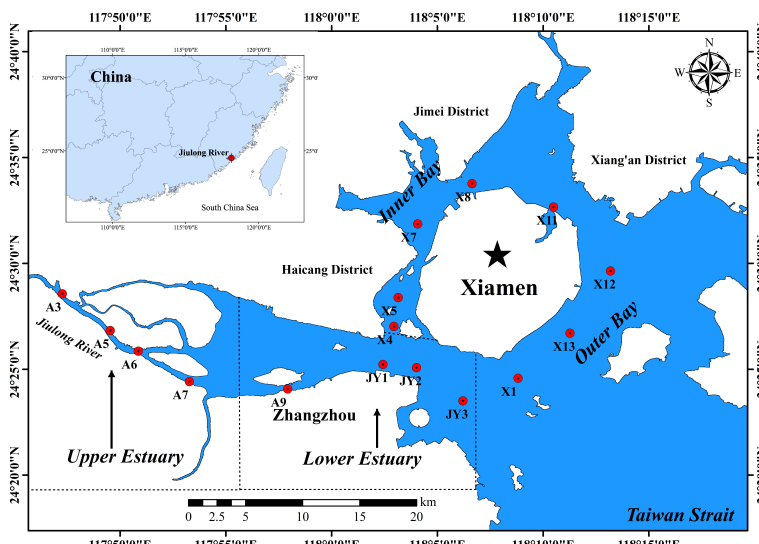

FIGURE 2

The geographic setting and sampling stations in the Jiulong River Estuary.

relatively stable (~ 32) in the bay area (stations of X1-X13). Water samples were stored in pre-cleaned polyethylene bottles once collected *via* using Niskin samplers with Tygon tubing. All the water samples for analyzing PPIX and its derivatives (chlorophyll-*a*, pheophytin and bacteriochlorophyll-*a*) were pre-screened through a 10 μm mesh to remove zooplankton and large particles, and then filtered through 0.7 μm GF/F filters. The filter membranes were immediately stored at –80°C once back in lab.

The water samples for analyzing dissolved inorganic nitrogen (DIN, including NO_3^-, NO_2^- and NH_4^+) and PO_4^{3-} were filtered using a 0.45 μm polycarbonate membrane (Millipore, USA), and analyzed later *via* the SEAL AutoAnalyzer 3 (Dai et al., 2008). The samples for analyzing particulate organic carbon (POC) and particulate nitrogen (PN) were collected using the GF/F filters (precombusted at 450°C for 4 h) and analyzed with a Vario EL cube elemental analyzer (Elementar, Hanau, Germany) after carbonates being removed with the fumes of concentrated HCl for 24 h (Liu et al., 2020). The abundances of autotrophic and heterotrophic microbial cells were determined *via* using the BD Accuri® C6 flow cytometry, once the samples were fixed by glutaraldehyde (final concentration 1%) at 4°C in the dark (Suffridge et al., 2018). The chlorophyll-*a* (Chl-*a*) and pheophytin concentrations in one aliquot of the water samples were determined using a Turner Designs Trilogy fluorometer according to the protocols in the Joint Global Ocean Flux Study (JGOFS) Core Measurements guide (Knap et al., 1996). Bacteriochlorophyll-*a* (BChl-*a*) was quantified at the wavelengths of 770 nm using HPLC according to the method of Goericke's (Goericke, 2002). Hydrological parameters, including salinity, water temperature, dissolved oxygen (DO), and pH, were measured *via* a portable water quality meter (WTW Multi 3430, Germany) on board.

The other aliquot of samples for PPIX were processed according to the procedure for chlorophyll *a* described in the JGOFS protocol, and all the samples were protected from light as much as possible during being processed (Knap et al., 1996). The PPIX molecules were extracted after the filters being soaked in 5.0 mL of 100% acetone and gently shaken for a few seconds. The samples in tubes were then wrapped in aluminium foil to avoid photo-degradation and then stored at –20°C for 20 h. Once done, 0.5 mL of the solvent was pipetted with 0.1 mL 1.2 M hydrochloric acid (v/v, 5/1) at pH < 2, and the acidification took place in the dark at room temperature for 24 h. The final solution was then quantified *via* HPLC after being filtered through a 0.45 μm polycarbonate membrane.

HPLC-MS analysis

PPIX in the samples was quantified *via* a Thermo Ultimate 3000 HPLC system (Dionex, California, U.S.A.) with a fluorescence detector. The chromatographic separation was performed through an InertSustain C18 column (4.6 × 150 mm, 5 μm, particle size), and the column oven temperature was set at 35 ± 1°C. A 12 min gradient flow was used with mobile phase A: 60% acetonitrile + 40% water + 0.1% formic acid and mobile phase B: 100% acetone + 0.1% formic acid (with all reagents of LC/MS grade). The flow rate was 1 mL/min and the injection volume was 100 μL. The linear gradient program was set as the following: 0 – 2 min: 20% B; 2 – 2.2 min: 100% B; 2 – 10 min: 100% B; 10 – 10.2 min: 20% B; and 10.2 – 12 min: 20% B. The excitation and emission wavelengths were set at 406 and 635 nm, respectively. The structure of PPIX in several samples was further confirmed *via* an Agilent 1290 UPLC binary pump and Agilent 6490 triple-quadrupole mass spectrometer equipped with an electrospray ionization source system (Agilent Technologies, California, U.S.A.). The detailed setup parameters for the HPLC and ESI–MS/MS were listed in the Table 1.

Method validation: Limits of detection, limits of quantitation, and quality control

The PPIX stock solution was prepared in 6.0 M formic acid and maintained at 4°C. A linear calibration curve was plotted using the chromographic values from ten standard calibration solutions (1.0 – 1500.0 nM/L diluted in acetone) with triplicate injections. An exemplary calibration curve is shown in the Figure 3D with standard peak areas (y) against the concentrations (x) R^2 > 0.99. Quality control samples were prepared with the following concentrations: 0.5, 1.0, 5.0, and 60.0 nM/L. To determine the limits of detection (LOD) and quantitation (LOQ), the signal-to-noise (S/N) ratio is calculated from triplicate injections of the 0.2 nM PPIX standard solution. Here, the noise is defined as the standard deviation of the peak areas, and the signal, as the mean of the peak areas of the triplicate injections. The LOD and LOQ are defined as 3 and 10 times of the S/N ratio, respectively. The results show that the signal-to-ratio (S/N) is 3.8, and the LOD and LOQ are 3.8 ± 1.0 pM and 12.8 ± 3.3 pM, respectively.

The intra- and inter-daily determinations of spiked PPIX samples were conducted for quality control. Here, six replicates (n = 6) at four concentrations were used. The accuracy is reflected by the percentage of measured concentration compared to the true value, and precision is expressed as the relative standard deviation (RSD). Table 2 shows the accuracy and precision of the PPIX in seawater (n = 6). The samples with less PPIX (0.5 nM) showed with a lower precision in both intra- and inter-daily measurements (Table 2). The samples with more PPIX (1.0 – 60.0 nM) showed with higher precision, with the RSD values of 0.4 – 8.3% (for the intra-daily check) and 1.7 – 2.1% (for the inter-daily check), respectively. Both sets of the values were below 15%, suggesting of an acceptable repeatability

TABLE 1   Experimental setups of HPLC and ESI−MS/MS for measuring PPIX.

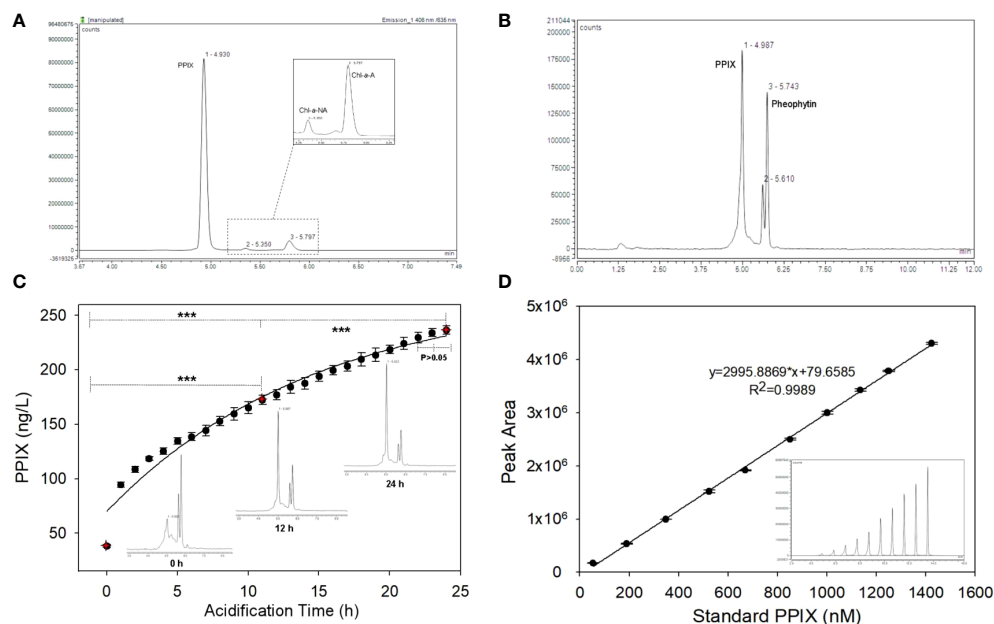| Ultimate 3000-HPLC			Agilent 6490 Triple-Quadrupole Mass Spectrometer		
Chromatographic conditions			**Electrospray conditions**		
Column dimensions 4.6 × 150 mm			Ionization mode		ESI [+]
Stationary phase C-18			Capillary voltage		3000 V
Particle size 5 µm			Source temperature		250°C
Mobile phase A	60% Acetonitrile + 40% Water + 0.1% Formic Acid		Sheath gas temperature		350°C
			Sheath gas flow		11 L/min
Mobile phase B	100% Acetone + 0.1% Formic Acid		Nebulizer gas		30 psi
			MS1/MS2 heater temperature		100°C
Column temperature 35 ± 1°C			Dwell time		80 ms
Autosampler temperature 4 ± 1°C			MS/MS		MRM
Flow rate	1 mL/min				
Injection volume	100 µL		Compounds	Transition	Collision energy
Linear gradient program			PPIX	563 > 504	46
Time (min)	A	B		563 > 489	55
0	80%	20%		563 > 445	56
2	80%	20%	Pheophytin a	872 > 593	44
2.2	0%	100%		872 > 533	46
10	0%	100%			
10.2	80%	20%			
12	80%	20%			

FIGURE 3
(A) The chromatogram of standard PPIX, Chl-*a* (pheophytin-*a*) and BChl in a mixed standard sample; (B) The HPLC chromatogram of PPIX in a seawater sample; (C) The variation of PPIX signals in a series of samples along with increasing acidification time (Inset: the chromatograms at 0, 12 and 24 h; *** denotes that $p < 0.001$ and the error bar represents the relative standard deviation of the analytes, n=5); (D) The exemplary calibration curve of PPIX (in peak area) at 10 different levels (Inset: the offset chromatogram of ten peaks; and the error bar refers to the relative standard deviation, n=3).

TABLE 2 The accuracy, precision, and stability of the determination of PPIX in seawater (n = 6).

Conc.(nM)	Intra-Day		Inter-Day		Stability (± SD%)			
	Accuracy (± SD%)	Precision (± SD%)	Accuracy (± SD%)	Precision (± SD%)	Day 4	Day 8	Day 14	Day 21
0.5	80.0 ± 4.6	14.4 ± 0.6	90.8 ± 11.7	4.6 ± 3.9	101.6 ± 4.4	108.3 ± 3.2	108.3 ± 6.3	108.9 ± 4.8
1	88.6 ± 3.1	3.6 ± 3.6	97.7 ± 10.6	2.1 ± 1.2	106.9 ± 6.8	99.9 ± 13.0	102.5 ± 6.9	104.8 ± 2.9
5	85.9 ± 2.2	0.4 ± 0.2	97.0 ± 11.3	2.1 ± 1.4	108.0 ± 3.0	106.1 ± 2.6	105.2 ± 2.1	99.6 ± 2.1
60	95.0 ± 11.0	8.3 ± 8.0	98.9 ± 8.8	1.7 ± 1.1	102.8 ± 0.6	102.3 ± 2.2	96.5 ± 0.8	95.3 ± 2.7

(intra-daily precision) and reproducibility (inter-daily precision) of the method. To evaluate the recovery, the collected filter membranes were spiked with 1 nM/mL PPIX standard (and additional triplicate filter membranes without spikes as control), and then processed according to our method. Thus, the average recovery was calculated as 97.5 ± 1.9% (n = 3). To evaluate the extraction efficiency of acetone, a set of samples (n = 5) were extracted consecutively (with acetone from one time until 4 times), and accumulative chromatographic values were calculated. According to the accumulative data, PPIX reached with 97.9 ± 0.7% after first extraction (coefficient of variation: ~ 0.64%), and remained relative constant with more extractions. Such results indicate of one-step extraction with acetone as efficiently but with low laborious cost. We further checked the stability of the samples (with 4 known concentrations as measured initially) along with time as we determined the PPIX contents in samples after 4, 8, 14, and 21 days (n = 6) (stored at 4°C). The data obtained at the later time were consistent with the original concentrations with the stabilities of 95 to 108% (the ratio of the later measurement to the original) (Table 2). Here, our results indicate that the collected filter membranes could be kept at 4°C for at least 21 days with no significant loss of PPIX.

Results

HPLC-ESI MS/MS analysis

The determination of PPIX extracted from water samples is summarized as follows. PPIX was quantified *via* HPLC at the excitation wavelength of 406 nm and emission wavelength of 635 nm, and the retention time of 4.7 to 5.2 min. The PPIX molecules are hydrophobic in structure with two peripherally ionizable propionate groups. The compound tends to be easily dissolved in organic solvent under acidic or basic conditions (Junga et al., 2010; Hoseini et al., 2019). Espinas et al. reported that the extraction efficiency of plant porphyrin strongly depended on the pH values as pH affects the solubility, the

aggregation and fluorescence intensity of PPIX (Espinas et al., 2012). Here, we used acetone to extract porphyrin from the samples for it not being destroyed as much as possible. On the other hand, the pigments including Chls and BChls in the other aliquot of samples were extracted simultaneously for subsequent analyses. It has been reported that the absorption peak for monomer PPIX was at 406 nm at pH < 2; a broad absorption peak appeared as an intermediate at 352 ~ 450 nm at pH of 3 to 7; a absorption spectrum was at 382 nm at pH > 8 (with dimer PPIX formed) (Hoseini et al., 2019). In fact, PPIX in organisms exists as in free forms, or as covalently and non-covalently bound to other ligands. Therefore, the sufficient acidification is required for converting all the PPIX forms to monomers (Espinas et al., 2012; Fyrestam et al., 2015).

The target peak of PPIX in the chromatogram was also identified along with Chl-*a* and BChl-*a*. The chromatogram (Figure 3A) shows with signals of standard PPIX, acidic Chl-*a* (pheophytin-*a*) and BChl-*a*. Here, the peaks of PPIX, Chl-*a* and pheophytin-*a* were clearly demodulated, but the BChl-*a* signal cannot be measured. This might be due to the concentration being too low or the signal intensity of PPIX too high at the excitation wavelength, which obscured the signal. The chromatogram of organic compounds extracted from the samples (Figure 3B) shows with the three distinct peaks at retention times of 4.9, 5.6, and 5.7 min, respectively. The target and standard PPIX appeared at an identical retention time of 4.9 min, whereas that of pheophytin was at 5.7 min. The structure of the PPIX molecules in the extracted samples was further confirmed based on the corresponding MS/MS ion spectra of their fragmented products. Previous researchers suggested of a primary fragmentation pathway of PPIX (Fyrestam and Östman, 2017). Our MS/MS analyses shows that the PPIX $[M + H]^+$ ions at *m/z* 563 formed the product ions at *m/z* 504, 445, and 489 (see Figure S1). The PPIX was accordingly characterized with these specific MS/MS product ion spectra (see Figure S1). Benzylic cleavage, with the loss of one (563 – 59) and two (563 – 2 × 59) –CH_2COOH groups, made PPIX forming the product ions at *m/z* 504 and 445,

respectively, which is again referred to as primary fragmentation pathway. The ion spectrum at m/z 489 here refers to the primary fragmentation product after the loss of a $-CH_2CH_2COOH$ group and proton (563 – 73 – 1), and the peak at m/z 489 might be derived from the ion at m/z 504 after the loss of a $-CH_3$ radical from later protonated ions (504 – 15). Accordingly, the results show that the PPIX targets could be detected according to their fragmentation products.

To evaluate the effects of acidification time on the measurements, a series of samples were acidified continuously for 24 h at ~ 25°C (lab temperature), and five samples were taken for analysis at each acidification time (Figure 3C). The chromatograph shows that the PPIX concentrations increased gradually with increasing acidification time, and the PPIX signals appeared to be well separated throughout (see the inserts in the Figure 3C). Apparently, the PPIX levels at different acidification time showed with significant differences (the levels at 12 h vs 0 h, $p < 0.001$; 24 h vs 12 h, $p < 0.001$). The kinetics of acidification was shown in the plot of all PPIX levels against acidification time, which was fitted with a first-order rate equation ($R^2 > 0.9699$; see Figure 3C). We therefore calculated that the acidification rate was ~ 0.0675 h^{-1} and the half time of forming PPIX monomers was ~ 4.4 h. No significant difference between signals at 22 h and 24 h ($p > 0.05$) indicates that measurements tends to be stable after ~ 24 h acidification. It should be noted that, based on the first-order acidification equation, 24 h acidification still rendered an underestimation of < 5% of the measurements. Finally, the newly developed protocol could be summarized as below: PPIX in cells is first extracted in acetone at -20°C for 20 h, and then adjusted to pH < 2, and the extracted samples are finally acidified in the dark for 24 h prior to being analyzed *via* HPLC.

The PPIX dynamics from the freshwater to saline waters

With the method, we measured cellular PPIX in the samples taken from the Jiulong River estuary. A total of 32 samples in 16 stations (surface and bottom) were collected from the upper to lower estuaries until the bay area. The results (Figure 4) show that the cellular PPIX concentrations in water samples ranged from 20 to 170 ng/L, with a decreasing pattern from the upper to lower estuaries until the bay waters. In the upper reaches of the upper estuary, PPIX (Figure 4A) was higher in the surface samples (140 ~ 170 ng/L) than in the bottom samples (60 ~ 140 ng/L) (Figure 4B), while in the lower estuary and inner bay waters, PPIX showed with higher concentrations in the bottom waters (40 ~ 100 ng/L) than in the surface waters (30 ~ 50 ng/L). In the outer bay waters, the concentrations of PPIX have no significant difference between the surface and bottom samples (except the station of X11).

PPIX has been previously measured in microbial pure cultures, with the average concentrations of 286, 214, and 2 ng/g in the cells of *Aggregatibacter actinomycetemcomitans*, *Porphyromonas gingivalis*, and *Saccharomyces cerevisiae*, respectively, accounting for 55%, 87%, and 1% of total porphyrins, respectively (Fyrestam et al., 2015). Our results show with the dynamics of PPIX in different waters, which could be attributable to the fact that microorganisms have differences in synthesizing and secreting PPIX. In particular, we for the first time quantified the cellular PPIX in the samples taken from natural waters with a high recovery rate and extraction efficiency, compared with the existing methods (Hur et al., 2014; Fyrestam et al., 2015; Fyrestam and Östman, 2017), our method is simpler and more efficient, and the method is expected to have a wider application in aquatic sciences.
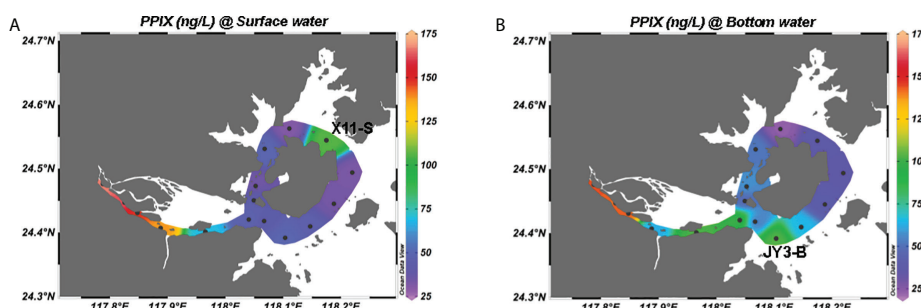

FIGURE 4
Spatial distributions of cellular PPIX in the Jiulong River estuary: **(A)** in the surface water; **(B)** in the bottom water.

Discussion and ecological relevance of PPIX

Tetrapyrroles are initially synthesized from a common precursor δ-aminolevulinic acid (ALA), and then form a series of metabolites including hemes, chlorophylls, vitamin B_{12}, siroheme, cofacter F_{430}, and porphyrins. As an essential metabolic intermediate, PPIX (with a cyclic tetrapyrrole core structure) is crucial in many biological processes including photosynthesis, respiration, methanogenesis, the assimilation and metabolism of inorganic nitrogen and sulphur (Senge et al., 2014). As PPIX is synthesized through multiple steps, the levels of PPIX in cells might be subject to vary depending on the cellular metabolic activities and ambient conditions. In a natural ecosystem, any disturbance in the PPIX levels might be further linked to changes in the ecological biodiversity and community structure.

Here, we measured cellular PPIX in the water samples taken from the Jiulng River estuary with acetone extraction and HPLC–MS/MS quantification. Firstly, our results show with different chromographic signals of PPIX at different acidification conditions. The sample (at pH < 2) has one single chromographic peak of PPIX; The sample (at pH of 3 ~ 7) has double peaks; The sample (at pH > 7) didn't show clear target peak (Figure S2). Secondly, we optimized the acidification time by conducting a time-series experiment. The separation of the PPIX signals was improved with increasing acidification time (Figure 3C). As there exist numerous metalloporphyrins (i.e., Fe-PPIX, Mg-PPIX and Zn-PPIX), the structures of these metalloporphyrins differ depending on their associated central metal ions, which might lead to a variable rate at which protons replace metal ions to form PPIX monomers (Fleischer, 1970; Yang et al., 2021). Besides, metalloporphyrins are also unstable according to their associated ions, likely following an order of stability as the following: medium–sized metals (like Fe^{2+}, Cu^{2+}, Zn^{2+}) > large sized metals (Hg^{2+}, Pb^{2+}, Cd^{2+}) > alkali metals (Na^+, K^+, Li^+) (Yang et al., 2021). For example, Cu^{2+} is more stable as a soft Lewis acid once tightly bound to porphyrin rings, which can only be desorbed or destructed under drastic conditions (Yang et al., 2021). The metalloporphyrins with large metals and alkali metals could be more easily transformed into the corresponding free porphyrin molecules in dilute acids (Barnes and Dorough, 1950; Yang et al., 2021). Here we confirmed that an acidification time of 24 h is sufficient for the dissociation of most metalloporphyrins and no destruction of their structures.

The Jiulong River is a typical subtropical macrotidal estuary with a depth of 3-16 m and its mean annual tidal range was 3.9 m with a maximum of 6.4 m (Yu et al., 2019). The freshwater inflow from the river and tidal intrusion from the Taiwan Strait together made the estuary with an obvious salinity gradient ranging from 0 to 32 in the upper to lower portions of the estuary (Figure S3) (Yu et al., 2020). Tidal intrusion leads to the water column more stratified in the lower estuaries (Yu et al., 2019). The plot of PPIX against salinity showed with a consistently decreasing pattern in the estuary ($p < 0.01$; Figure 5A). As described previously, the study area is divided into two sections: the estuary and the bay. The estuary includes the stations of A3 to JY1, with a salinity range of 2 to 26 (Figure S3). Here, the concentrations of PPIX decreased with increasing salinity, with a significantly negative correlation ($p < 0.01$). The bay area (JY2-X13) exhibited with a salinity range of 27 to 32, and no significant correlation was observed between PPIX and salinity ($p > 0.05$). It should be noted that a few outliers (at JY3-B and X11-S) occurred in the Bay waters. The Jiulong River received a large quantity of organic matter and nutrients from the upper streams, storm water, and even domestic sewages, which in turn triggered the growth and reproduction of microorganisms and phytoplankton locally (Chen et al., 2018; Yu et al., 2020). Higher levels of PPIX at the upper reaches of the upper estuary in this study could be attributable to the higher riverine nutrient inputs and associated higher algal and bacterial activities. In the lower estuary (with a maximum width of approximately 100 km^2, the water flow rate decreased and water retention time increased. Under such conditions, suspended particles are subject to deposit, and algae tend to grow easily with increased sunlight (Sullivan et al., 2001; Zeng et al., 2006). The higher concentrations of PPIX in the bottom waters of the lower estuary (Figure 4) might be associated with the resuspension and dissolution of the deposited particles and organic materials.

The ambient environment could be critical affecting the levels of cellular PPIX. We therefore statistically analyzed the samples taken from stations of JY2-X13 with similar salinity of ~ 30 to minimize the effects of salinity (excluding the stations [blue dots] with lower salinity in the Figure 5A). As PPIX is highly involved in the metabolic processes in microbes, we first plotted the cellular PPIX dynamics against the autotrophic and heterotrophic microbial cells. The abundances of autotrophic microbes were higher in the surface waters than in the bottom of the Jiulong River estuary (Figure S3), and especially in the upper estuary and inner bay waters, which might be attributable to the fact that the autotrophic organisms could receive sufficient sunlight in surface for photosynthesis (Kolber et al., 2000). The bacterial abundances were higher in the bottom waters than in the surface waters in the estuary, probably as a result of more organic matter accumulation there. We did not observe any consistent pattern of cellular PPIX against autotrophic and bacterial abundances (Figure 5B, $p > 0.05$), and here further experiments are needed for elucidating possible connections between PPIX with biological activities. Chlorophylls are the most abundant and noticeable biological pigments in virtually all the photosynthetic organisms, including all the higher plants, green algae and cyanobacteria (Grimm et al., 2006). Through photosynthesis in chlorophylls, the solar energy was converted into chemical energy. Therefore chlorophylls can be used as an indicator of the photosynthetic potential and primary production

(Senge et al., 2014). The biosynthetic pathway of chlorophyll involves a branch of non-metallized PPIX in which one Mg^{2+} ion is inserted in the center of the porphyrin ring catalyzed by ATP-dependent Mg-chelatase (Chen et al., 2018). Thereafter, the Mg-PPIX experiences a series of reactions leading to the syntheses of chlorophyll and bacteriochlorophyll. Pheophytin is a compound formed by the degradation of chlorophyll, by the action of weak acids or enzymes, where Mg^{2+} is replaced by two hydrogen atoms (pheophytin *a* and pheophytin *b* are derived from chlorophyll *a* and chlorophyll *b*, respectively) (Hsu et al., 2013). Therefore, the relationships between PPIX and the three biopigments (Chl-*a*, pheophytin and BChl-*a*) might be used as an indicator of the status of environmental microbial communities. We plotted the ratios of PPIX/Chl-*a*, PPIX/BChl-*a*, and PPIX/Pheophytin as biological variables against the concentrations of PPIX to exposit the variation of PPIX content per unit biomass. The results (Figure 5C) show a significant positive correlation ($p < 0.05$) between PPIX and the three pigments. Except for the surface sample at X11, all the three ratios increased with increasing PPIX concentrations in the high-salinity waters (Figure 5C). Such results indicated of a close interaction between PPIX and the three biopigments. Interestingly, the three ratios in the bottom samples were

greater than those in the surface water. It is possibly related to the fact that the bottom waters contained higher levels of organic matter and nutrients. In addition, the surface waters might be exposed to excessive sunlight leading to a photoinhibition effect on photosynthetic microorganisms (as the samples at A9-JY3, X1-X7 were collected at 12:30 - 16:30 pm) (Jiao et al., 2010), with possible degradation of free PPIX under light. As a metabolite in the biosynthetic pathway of chlorophylls, PPIX could be an important indicator of the growth status of photosynthetic organisms.

Nutrients (including N and P as backbone elements in biology) are traditionally believed to be crucial in dictating planktonic biomass, taxonomic composition and primary production (Smith, 2003). Low concentrations of nutrients (below the threshold) restricted the growth rate of primary production and autotroph biomass; and conversely, excessive concentrations could lead to ecological disturbances including harmful algal blooms, hypoxia and the production of toxins (Wilkinson, 2017). The Jiulong River estuary receives a large amount of particles from both riverine inputs and adjacent urban sewages (Cao et al., 2005). As a result, the concentrations of POC and PN showed with a gradually decreasing pattern from the upper to lower estuaries (Figure S3). Specifically,
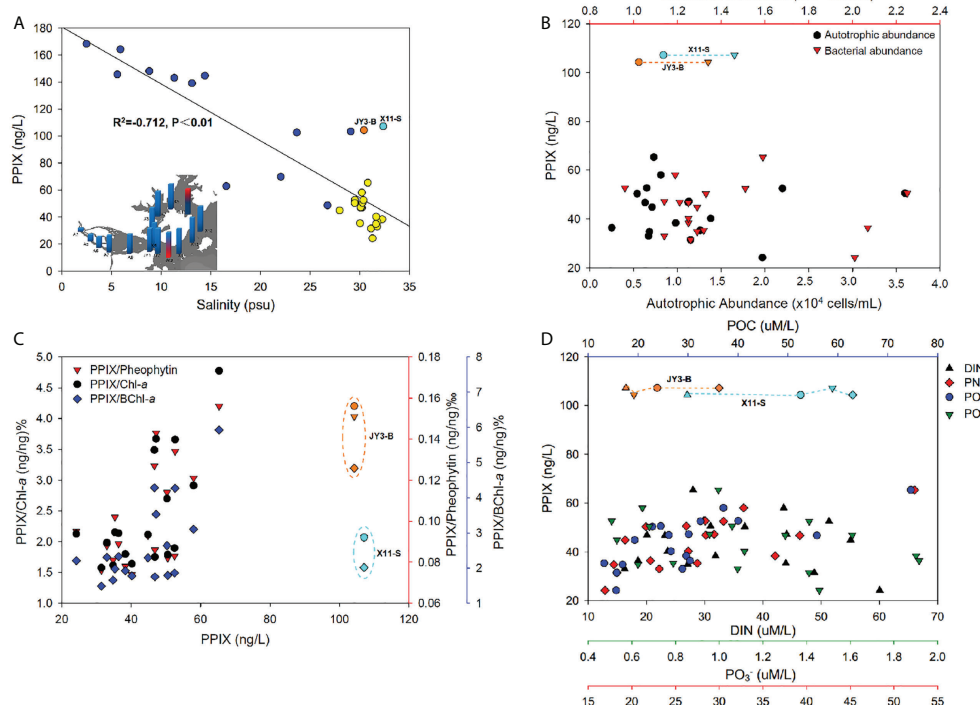

FIGURE 5
(A) The negative correlation of PPIX concentrations against salinity (the inset refers to the salinity distribution, the red marks denoted the outliers of PPIX that responded to JY3-B (orange dot) and X11-S (light blue dot), and the yellow dots referred to the high salinity samples). **(B)** The relationship of PPIX with the autotrophic and bacterial abundances. **(C)** The variations of PPIX/Chl-*a* (black dots), PPIX/BChl-*a* (blue diamonds) and PPIX/Pheophytin (red triangles) along with PPIX. **(D)** The synergistic changes of PPIX with the DIN (black triangles), PN (red diamonds), POC (blue dots) and PO_4 (3−) (green triangle down) concentrations.

increased levels of POC and PN occurred at the bottom near the river mouth as a result of particle inputs and resuspensions there. Similar decreasing trends were found for the nitrate, nitrite, ammonium, and phosphate levels, with extremely high levels at the river mouth (Figure S3). In particular, the cellular PPIX concentrations were significantly positively correlated ($p < 0.01$) with POC and PN in those high-salinity waters (see Figure 5D), but no significantly linear correlations of PPIX with DIN and phosphate ($p > 0.05$). Instead, PPIX varied dynamically along with DIN and phosphate: PPIX increased slightly with increasing DIN and phosphate, and then decreased (Figure 5D). This could be attributable to the biological quotas of PPIX were relatively stable, and increased nutrients will not necessarily trigger more PPIX synthesis beyond the quota. It should be noted here that more researches are required to confirm the conclusion. Consistently, the stations of JY3-B showed with unusually high PPIX values (Figures S3, 5A), which was located in the estuary-ocean interface with high POC and PN, but low DIN and phosphate.

The Jiulong River estuary is partially stratified particularly in the lower portion (Yu et al., 2019). The JY3 sample was collected at 16:30 pm, near a neap tide and the salinity in the bottom waters was at least > 1 higher than in the surface waters. Consistently, Zeng et al. (2006) reported that the phytoplankton abundances were significantly negatively correlated with the nitrate, nitrite and phosphate levels in the Xiangxi River (one of the upper branches in the Three Gorges, Yangtze River). Previous researchers reported that the abundances of primary plankton groups (diatoms, cryptophytes, chlorophytes and cyanobacteria) were negatively correlated with the nitrate and phosphate levels in the Jiulong River estuary (Xie et al., 2018). In addition, sediment suspension in the water column could provide extra nutrients for the growth of particle-attached microorganisms, while the degradation of organic matter could further provide logistical support for the growth of free-living microorganisms (Li et al., 2021). Consequently, microbial activities commonly become more intense in places with high levels of particulate organic matter, possibly leading to accelerated metabolism and increased PPIX syntheses. Figure 4 shows that PPIX were higher in the upper estuary (A3-A7 stations), while relatively lower in the lower estuary, and lowest at the outer bay waters (Figures S3, 5D). At the stations of A9-X1 near the river mouth, the PPIX contents in the bottom samples were significantly higher than in the surface samples, which was consistent with higher particle organic matter there. It is worthy to note that the station of X11 also revealed a high PPIX level at surface (Figure 4), as directly receiving materials' input from a lagoon nearby. The highest and lowest PPIX concentrations (168 and 24 ng/L) occurred in the samples taken from the stations of A3 and X8, respectively. The station A3 is located at the river mouth with the highest nutrient levels (Yu et al., 2019).

Conclusion

In this study, we developed a new technique for the determination of PPIX in natural waters, and then successfully applied it to quantify the contents of PPIX in seawater samples took from a subtrophic estuary-the Jiulong River estuary. We for the first time linked PPIX with natural ecosystems, and explored the intrinsic factors that affect the construction and diversity of microbial communities. Generally, we obtained a first dataset of PPIX in a coastal system and further discussed the potential significance of PPIX in the system. In particular, a significantly negative correlation was observed between PPIX and salinity, and a positive correlation of PPIX with downstream derivatives (the three biopigments: Chl-*a*, pheophytin and BChl-*a*) and particulate organic substances (PN and POC). In addition, we observed that PPIX varied dynamically with increasing levels of nutrients (DIN and phosphate), indicative of the association of PPIX with the growth of phytoplankton and bacteria. Our findings emphasized the ecological functioning of PPIX as a natural bioorganic molecule in natural waters. The technique and findings might shed light on our further understanding on the structure of microbial communities, and the cycling of nutrients in natural ecosystems. Future studies should focus on biological data such as those from high-throughput sequencing and metagenome or meta-transcriptomics analyses.

Data availability statement

The original contributions presented in the study are included in the article/Supplementary Material. Further inquiries can be directed to the corresponding author.

Author contributions

The methods described in this paper were developed by LG with support and guidance from DW. All the experiments and the manuscript preparation were performed by LG. KM helped with the experiment and manuscript writing. XY helped collecting the samples and analyzing the data. HZ helped plotting the figures. The manuscript was reviewed by LG, and substantially revised by DW. All authors contributed to the article and approved the submitted version.

Funding

Acknowledgments

Conflict of interest

The authors declare that the research was conducted in the absence of any commercial or financial relationships that could be construed as a potential conflict of interest.

Publisher's note

All claims expressed in this article are solely those of the authors and do not necessarily represent those of their affiliated organizations, or those of the publisher, the editors and the reviewers. Any product that may be evaluated in this article, or claim that may be made by its manufacturer, is not guaranteed or endorsed by the publisher.

Supplementary material

The Supplementary Material for this article can be found online at: https://www.frontiersin.org/articles/10.3389/fmars.2022.991126/full#supplementary-material

References

Ausio, X., Grimalt, J. O., Ozalla, D., and Herrero, C. (2000). On-line LC-MS analysis of urinary porphyrins. *Analytical Chem.* 72 (20), 4874–4877. doi: 10.1021/ac0005060

Baohong, C., Kang, W., Xu, D., and Hui, L. (2021). Long-term changes in red tide outbreaks in xiamen bay in China from 1986 to 2017. *Estuarine Coast. Shelf Sci.* 249, 107095. doi: 10.1016/j.ecss.2020.107095

Barnes, J. W., and Dorough, G. D. (1950). Exchange and replacement reactions of α,β,γ,δ-Tetraphenyl-metalloporphins1. *J. Am. Chem. Soc.* 72 (9), 4045–4050. doi: 10.1021/ja01165a057

Bonkovsky, H. L., Guo, J. T., Hou, W., Li, T., Narang, T., and Thapar, M. (2013). Porphyrin and heme metabolism and the porphyrias. *Compr. Physiol.* 3 (1), 365–401. doi: 10.1002/cphy.c120006

Cao, W., Hong, H., and Yue, S. (2005). Modelling agricultural nitrogen contributions to the jiulong river estuary and coastal water. *Global Planetary Change* 47 (2), 111–121. doi: 10.1016/j.gloplacha.2004.10.006

Chen, G. E., Canniffe, D. P., Barnett, S. F. H., Hollingshead, S., Brindley, A. A., Vasilev, C., et al. (2018). Complete enzyme set for chlorophyll biosynthesis in escherichia coli. *Sci. Adv.* 4 (1), eaaq1407. doi: 10.1126/sciadv.aaq1407

Chen, B., Kang, W., and Hui, L. (2019). Akashiwo sanguinea blooms in Chinese waters in 1998–2017. *Mar. pollut. Bull.* 149, 110652. doi: 10.1016/j.marpolbul.2019.110652

Chen, N., Krom, M. D., Wu, Y., Yu, D., and Hong, H. (2018). Storm induced estuarine turbidity maxima and controls on nutrient fluxes across river-estuary-coast continuum. *Sci. Total Environ.* 628-629, 1108–1120. doi: 10.1016/j.scitotenv.2018.02.060

Dailey, H. A., and Meissner, P. N. (2013). Erythroid heme biosynthesis and its disorders. *Cold Spring Harb. Perspect. Med.* 3 (4), a011676. doi: 10.1101/cshperspect.a011676

Dai, M., Wang, L., Guo, X., Zhai, W., Li, Q., He, B., et al. (2008). Nitrification and inorganic nitrogen distribution in a large perturbed river/estuarine system: The pearl river estuary, China. *Biogeosciences* 5 (5), 1227–1244. doi: 10.5194/bg-5-1227-2008

Danton, M., and Lim, C. K. (2006). Porphyrin profiles in blood, urine and faeces by HPLC/electrospray ionization tandem mass spectrometry. *BioMed. Chromatogr.* 20 (6-7), 612–621. doi: 10.1002/bmc.656

Datta, S., Loh, C., MacRobert, A., Whatley, S., and Matthews, P. (1998). Quantitative studies of the kinetics of 5-aminolaevulinic acid-induced fluorescence in bladder transitional cell carcinoma. *Brifsh J. Cancer* 78 (8), 1113–1118. doi: 10.1038/bjc.1998.637

De Maere, H., Jaros, M., Dziewięcka, M., De Mey, E., Fraeye, I., Sajewicz, M., et al. (2014). Determination of hemin, protoporphyrin ix, and Zinc(Ii) protoporphyrin ix in parma ham using thin layer chromatography. *J. Liquid Chromatogr. Related Technol.* 37 (20), 2971–2979. doi: 10.1080/10739149.2014.906995

Espinas, N. A., Kobayashi, K., Takahashi, S., Mochizuki, N., and Masuda, T. (2012). Evaluation of unbound free heme in plant cells by differential acetone extraction. *Plant Cell Physiol.* 53 (7), 1344–1354. doi: 10.1093/pcp/pcs067

Fleischer, E. B. (1970). Structure of porphyrins and metalloporphyrins. *Accounts Chem. Res.* 3 (3), 105–112. doi: 10.1021/ar50027a004

Fyrestam, J., Bjurshammar, N., Paulsson, E., Johannsen, A., and Ostman, C. (2015). Determination of porphyrins in oral bacteria by liquid chromatography electrospray ionization tandem mass spectrometry. *Anal. Bioanal Chem.* 407 (23), 7013–7023. doi: 10.1007/s00216-015-8864-2

Fyrestam, J., and Östman, C. (2017). Determination of heme in microorganisms using HPLC-MS/MS and cobalt(III) protoporphyrin IX inhibition of heme acquisition in escherichia coli. *Anal. Bioanal Chem.* 409, 6999–7010. doi: 10.1007/s00216-017-0610-5

Goericke, R. (2002). Bacteriochlorophyll a in the ocean: Is anoxygenic bacterial photosynthesis important? *Limnology Oceanog* 47 (1), 290–295. doi: 10.4319/lo.2002.47.1.0290

Grimm, B., Porra, R. J., Rüdiger, W., and Scheer, H. (2006). *Chlorophylls and bacteriochlorophylls: Biochemistry, biophysics, functions and applications* (The Netherlands: Springer). doi: 10.1007/1-4020-4516-6

Hoseini, M., Sazgarnia, A., and Sharifi, S. (2019). Effect of environment on protoporphyrin IX: Absorbance, fluorescence and nonlinear optical properties. *J. Fluoresc* 29 (3), 531–540. doi: 10.1007/s10895-019-02366-4

Hsu, C.-Y., Chao, P.-Y., Hu, S.-P., and Yang, C.-M. (2013). The antioxidant and free radical scavenging activities of chlorophylls and pheophytins. *Food Nutr. Sci.* 04 (08), 1–8. doi: 10.4236/fns.2013.48A001

Hur, Y., Han, S. B., Kang, S. W., and Lee, Y. (2014). Quantitative analysis of porphyrins in dried blood spots using liquid chromatography-tandem mass spectrometry with pre-column derivatization. *Bull. Korean Chem. Soc.* 35 (10), 3103–3106. doi: 10.5012/bkcs.2014.35.10.3103

Jiao, N., Zhang, F., and Hong, N. (2010). Significant roles of bacteriochlorophylla supplemental to chlorophylla in the ocean. *ISME J.* 4 (4), 595–597. doi: 10.1038/ismej.2009.135

Junga, C.-I., Yang, J.-I., Park, C.-H., Lee, J.-B., and Park, H.-R. (2010). *Formation of the metal complexes between protoporphyrin IX and divalent metal cations in the environment, molecular environmental soil science at the interfaces in the earth's critical zone, Berlin, Heidelberg, 2010.* Eds. J. Xu and Huang, (Berlin, Heidelberg: Springer Berlin Heidelberg) pp 97–99.

Jerry Kaneko, J. (1997). Chapter 8 - Porphyrins and the porphyrias. *Clin. Biochem. Domest. Anim. (Fifth Edition)*, Salt Lake City, Utah, USA, 1997. Eds. J. Jerry Kaneko, John W. Harvey and Michael L. Bruss, (Salt Lake City, Utah: American Academic Press) pp 205–221. doi: 10.1016/B978-012396305-5/50009-9

Knap, A. H., Michaels, A., Close, A. R., Ducklow, H., and Dickson, A. G. (1996). *Protocols for the joint global ocean flux study (JGOFS) core measurements* Vol. Measurement of Chlorophyll a and Phaeopigments by Fluorometric Analysis. Ed. A. G. Dickson (Paris, France: UNESCO-IOC) 119–122.

Kolber, Z. S., Van Dover, C. L., Niederman, R. A., and Falkowski, P. G. (2000). Bacterial photosynthesis in surface waters of the open ocean. *Nature* 407 (6801), 177–179. doi: 10.1038/35025044

Li, J., Gu, L., Bai, S., Wang, J., Su, L., Wei, B., et al. (2021). Characterization of particle-associated and free-living bacterial and archaeal communities along the water columns of the south China Sea. *Biogeosciences* 18 (1), 113–133. doi: 10.5194/bg-18-113-2021

Lim, C. K. (2009) High-performance liquid chromatography and mass spectrometry of porphyrins, chlorophylls and bilins. (United Kingdom: World Scientific Publishing, UK Ltd, UK). *Methods in Chromatography*. 2, 1–256.

Liu, Q., Liang, Y., Cai, W.-J., Wang, K., Wang, J., and Yin, K. (2020). Changing riverine organic C:N ratios along the pearl river: Implications for estuarine and coastal carbon cycles. *Sci. Total Environ.* 709, 136052. doi: 10.1016/j.scitotenv.2019.136052

Sachar, M., Anderson, K. E., and Ma, X. (2016). Protoporphyrin IX: The good, the bad, and the ugly. *J. Pharmacol. Exp. Ther.* 356 (2), 267. doi: 10.1124/jpet.115.228130

Senge, M., Ryan, A., Letchford, K., MacGowan, S., and Mielke, T. (2014). Chlorophylls, symmetry, chirality, and photosynthesis. *Symmetry* 6 (3), 781–843. doi: 10.3390/sym6030781

Smith, V. H. (2003). Eutrophication of freshwater and coastal marine ecosystems a global problem. *Environ. Sci. pollut. Res.* 10, 126–139. doi: 10.1065/espr2002.12.142

Stillman LC, G. M. (1978). Protoheme extraction from plant tissue. *Analytical Biochem.* 91 (1), 166–172. doi: 10.1016/0003-2697(78)90827-8

Suffridge, C. P., Gómez-Consarnau, L., Monteverde, D. R., Cutter, L., Arístegui, J., Alvarez-Salgado, X. A., et al. (2018). And their congeners as potential drivers of microbial community composition in an oligotrophic marine ecosystem. *J. Geophysical Research: Biogeosci.* 123 (9), 2890–2907. doi: 10.1029/2018JG004554

Sullivan, B. E., Prahl, F. G., Small, L. F., and Covert, P. A. (2001). Seasonality of phytoplankton production in the Columbia river: A natural or anthropogenic pattern? *Geochimica Cosmochimica Acta* 65 (7), 1125–1139. doi: 10.1016/S0016-7037(00)00565-2

Tian, J., Ge, F., Zhang, D., Deng, S., and Liu, X. (2021). Roles of phosphate solubilizing microorganisms from managing soil phosphorus deficiency to mediating biogeochemical p cycle. *Biology* 10 (2):158–177. doi: 10.3390/biology10020158

Wang, D., Lu, S., Chen, N., Dai, M., and Gueguen, C. (2018). Human perturbation increases the fluxes of dissolved molybdenum from land to ocean - the case of the jiulong river in China. *J. Environ. Manage* 210, 139–145. doi: 10.1016/j.jenvman.2017.12.074

Weinberger, R., and Sapp, E. (1990). Capillary electrophoresis of urinary porphyrins with absorbance and fluorescence detection. *J. Chromatogr.* 516, 271–285. doi: 10.1016/S0021-9673(01)90225-0

Weinstein JD, B. S. (1984). Biosynthesis of protoheme and heme a precursors solely from glutamate in the unicellular red alga cyanidium caldarium. *Plant Physiol.* 74 (1), 146–151. doi: 10.1104/pp.74.1.146

Wilkinson, G. M. (2017). "Eutrophication of freshwater and coastal ecosystems," in *Encyclopedia of sustainable technologies*, (Oxford, UK: Elsevier) pp 145–152.

Xie, Y., Wang, L., Liu, X., Li, X., Wang, Y., and Huang, B. (2018). Contrasting responses of intertidal microphytobenthos and phytoplankton biomass and taxonomic composition to the nutrient loads in the jiulong river estuary. *Phycological Res.* 67 (2), 152–163. doi: 10.1111/pre.12363

Xiong, J., Fu, G., Yang, Y., Zhu, C., and Tao, L. (2011). Tungstate: Is it really a specific nitrate reductase inhibitor in plant nitric oxide research? *J. Exp. Bot.* 63, 33–41. doi: 10.1093/jxb/err268

Yang, H., Zhou, Y., and Liu, J. (2021). Porphyrin metalation catalyzed by DNAzymes and nanozymes. *Inorganic Chem. Front.* 8 (9), 2183–2199. doi: 10.1039/D1QI00105A

Yu, D., Chen, N., Cheng, P., Yu, F., and Hong, H. (2020). Hydrodynamic impacts on tidal-scale dissolved inorganic nitrogen cycling and export across the estuarine turbidity maxima to coast. *Biogeochemistry* 151 (1), 81–98. doi: 10.1007/s10533-020-00712-4

Yu, D., Chen, N., Krom, M. D., Lin, J., Cheng, P., Yu, F., et al. (2019). Understanding how estuarine hydrology controls ammonium and other inorganic nitrogen concentrations and fluxes through the subtropical jiulong river estuary, S.E. China under baseflow and flood-affected conditions. *Biogeochemistry* 142 (3), 443–466. doi: 10.1007/s10533-019-00546-9

Zeng, H., Song, L., Yu, Z., and Chen, H. (2006). Distribution of phytoplankton in the three-gorge reservoir during rainy and dry seasons. *Sci. Total Environ.* 367 (2-3), 999–1009. doi: 10.1016/j.scitotenv.2006.03.001

Zvezdanovic, B. J., Petrovic, M. S., and Markovic, Z. D. (2017) Hematoporphyrin derivatives: The ultrahigh performance liquid chromatography: Diode array: Electrospray ionization: Mass spectrometry analysis. *Advanced technologies*. 6:26–30. doi: 10.5937/savteh1702026Z